Time-resolved single-shot revealing pulse evolution dynamics in ultrafast lasers

Tianhao Xian
Shanghai Jiao Tong University
Wenchao Wang
Shanghai Jiao Tong University
Li Zhan (lizhan@sjtu.edu.cn)
Shanghai Jiao Tong University https://orcid.org/0000-0002-0832-0354

Article

Keywords: LED, light sources, laser design

Posted Date: January 25th, 2021

DOI: https://doi.org/10.21203/rs.3.rs-148495/v1

Time-resolved single-shot revealing pulse evolution dynamics in ultrafast lasers

Tianhao Xian, Wenchao Wang, and Li Zhan*

Mode-locked lasers are the ideal source for precise measurements, from frequency combs to precise timing, which relies on the accurate control of the intracavity parameters in the lasers to stabilize the pulse. However, by the lack of accurate measurements, the interplays between intracavity parameters and the mode-locked pulse is still not real-time observable. Here, using the dispersive temporal interferometer, we report a method to single-shot probe the pulse evolution dynamics in time domain in the mode-locked laser. As a typical example, we demonstrate the first single-shot observation on the roundtrip time and phase evolutions of intracavity pulse during its buildup and relaxation. Three distinct evolution regimes for pulse buildup are unveiled for the first time. Moreover, the physical mechanism of the time-location and phase changes in these three regimes has also been analyzed, respectively. Our researches present a novel method to observe the intracavity-parameters-to-pulse interaction, which will improve laser design, ultrafast diagnostics, and nonlinear optics.

State Key Laboratory of Advanced Optical Communication Systems and Networks, School of Physics and Astronomy, Shanghai Jiao Tong University, Shanghai 200240, China. * Correspondence and requests for materials should be addressed to L. Z. (email: lizhan@sjtu.edu.cn)

Ultrafast lasers[1] have developed rapidly over the past decades, owing to their comprehensive applications in many areas such as precise timing[2], frequency comb[3], photonic switching[4], sensor and biomedicine[5]. The efficient mean to generate ultrashort pulses is to utilize mode-locking, in which a large number of longitudinal modes are locked together in the same phase to form the ultrashort pulse, even short down to few optical cycles[6,7]. In mode-locked lasers, the ultrafast pulses arise from the balance of the energy exchange between the laser and the environment with the presence of nonlinearity and dispersion[8]. The interplays between the pulse and the cavity parameters are of particular interest in mode-locked lasers because they unveil a lot of pulse dynamics[9]. Reciprocally, to observe such dynamics is of great importance to improve the performance of ultrafast lasers.

Although the dynamics of mode-locked lasers have been extensive investigated theoretically[10, 11], experiment has been mitigated and the time-resolved measurement is often restricted to use fast photodetectors[12]. Recently, with the introduction of the dispersive Fourier transform (DFT) to real-time observe the pulse spectrum[13], different phenomena in mode-locked lasers have been observed, such as the mode-locking buildup[14, 15], soliton molecules[16,17], soliton explosion[18,19], and breather soliton[20]. These studies have vastly promoted human's understanding on optical solitons, and unambiguously stimulated the development of ultrafast lasers. However, limited by the capability of DFT technique, soliton dynamics is observed in the spectral domain only. The observation of intracavity factors, which may affect the roundtrip time or the soliton phase, are beyond the capability of DFT technique. Whereas, to understand the interactions between mode-locked pulses and the laser components, the evolutions of pulse location (roundtrip time) and phase over roundtrips should be single-shot investigated. Furthermore, due to its extensive applications in few-cycle pulse generation[21], femtosecond pulse synthesis[22], frequency comb[23], and precise timing[24], it is of the essence for the mode-locked lasers to deliver pulses with high stable envelope phase and/or pulse location (roundtrip time or repetition frequency). Hence, to time-resolved understand the mode-locked lasers is not only of great importance in fundamental science, but also attractive for practical applications.

Here, by means of an emerging ultrafast time-resolving technique, the dispersive temporal interferometer (DTI), we propose the single-shot resolving of the pulse-to-pulse and pulse-to-cavity interactions of ultrafast laser. We reveal the evolutions of relative pulse location (roundtrip time) and phase during the buildup and relaxation process of mode-locking. Experimentally, we find that the seed fluctuation sees a rapid acceleration as it transforms into mode-locked pulse. Additionally, three-stage relaxation, namely soliton breath, relaxation oscillation, and long-term relaxation, is unveiled for the first time. Theoretically, we propose that the gain depletion accelerates the pulses, and analyze the influences of gain and the refractive index change to the laser. These discoveries can enhance the understanding on the dynamics of mode-locked laser, and help to fabricate high stable ultrafast lasers for optical frequency comb and precise timing.

Results

Monitoring pulse-to-pulse interaction using DTI. The concept of DTI comes from the temporal analogy of the spatial double-slit interference[25], in which the light is split by two parallel slits off two coherent parts, and the interference fringes arise on the screen far from the slits. As its temporal projection, the DTI splits the ultrashort pulse into two paths and then reassemble them into a pulse pair with time separation τ. The pulse pair serves as the temporal double-slit and τ is their distance. The analogy to diffraction propagation is implemented by large dispersion in DTI, after which the interference arises in time-domain and the interferogram can be captured by oscilloscope. This method was firstly proposed to monitor the time signal imposed on the paths, which can probe the time difference from attosecond to picosecond with sub-20as resolution[26]. Here, we introduce the DTI technique to mode-locked laser and employ it to capture the pulse-to-pulse and pulse-to-cavity-parameters interactions in ultrafast lasers.

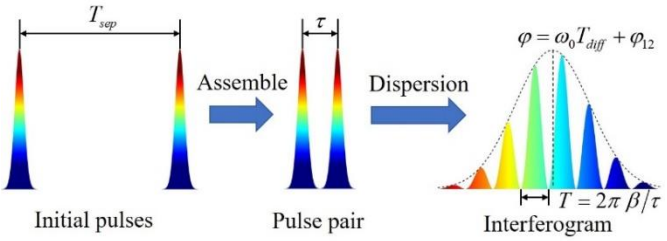

Fig. 1. Concept of capturing the interaction of different pulses with DTI.

The concept of using the DTI to capture the relation of different pulses is sketched in Fig. 1: two separated pulses is firstly assembled into close-spaced pulse pair, and then stretched with large dispersion to encode their time separation τ and relative phase φ_{12} into the temporal interferogram. This requires the former pulse undergoes a long distance than the latter in the separate paths, which induces a time difference T_{diff} that fulfills $\tau = \pm\left(T_{sep} - T_{diff}\right)$, where T_{sep} is the separation of two pulses. After the DTI, the interferogram writes as:

$$I(t) \approx (1/\beta)\left|E(\omega)\right|^2\left[1+\cos\left(\tau t/\beta + \omega_0 T_{diff} + \varphi_{12}\right)\right] \qquad (1)$$

where β is the total dispersion, ω_0 refers to the carrier frequency, and $E(\omega)$ represents the Fourier transform of the envelop of the pulse. Here, we should point out that the two pulses are treated as identical solitons for simplicity.

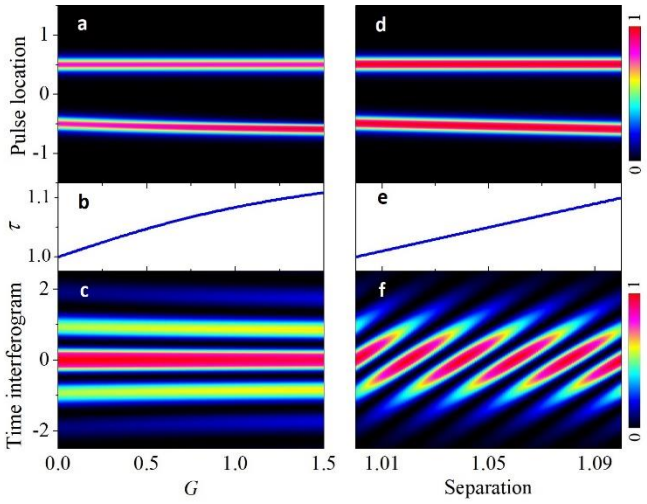

Fig. 2. Time shift of mode-locked pulses due to time-dependent gain (left panel) and refractive index change (right panel). **a(d)** pulse relative location. The upper is the reference pulse that has a fix location, and the lower is the signal pulse. **b(e)** relative time separation of the pulses in **a(d)**. **c(f)** time interferogram evolution of the pulses in **a(d)**.

Since the characterization of soliton-soliton interplays is based on the interference of the two solitons, it is instructive to present the correspondence between the origin of pulse temporal shift and the interferogram. In mode-locked lasers, the parameters that affect the pulse location are mainly refractive index and gain depletion[27, 28]. The change of the former mainly comes from Kerr

effect[13, 15], the Kramers-Krönig (KK) relation[29]. The Kerr effect can slow down the pulse through increasing the momentary refractive index of the fiber[30]. According to the KK relation, the change of population inversion of gain medium will reform its refractive index, and then change its relative location.

The gain depletion theory was firstly introduced to model the slow saturable absorber mode-locked laser in 1975[31], and has been employed to explain the pulse-to-pulse interaction in the lasers[32]. As the lifetime of gain medium is much larger than the pulse duration, the energy that transferred to the pulse cannot be replenished immediately, which introduces a gain depletion during the pulse passing. Therefore, the tail of the pulse sees smaller gain than the front, and the net gain of the pulse in a roundtrip is[27]:

$$g_{\text{net}}(t) = G\left(1 - \frac{2}{E_s}\int_{-\infty}^{t} |a(t')|^2 dt'\right) \quad (2)$$

where G measures the magnitude of the depletion that occurs during pulse interaction, E_s refers to the pulse energy and $a(t)$ is the pulse envelop. Fig. 2a presents the pulse location when exerted different gain depletion and Fig. 2b is the time separation of signal pulse and the reference pulse. As the increase of G, the time separation increases, exhibiting that the pulse moves forward. Here, we simulate the time interferogram of these two pulses using DTI (Fig. 2c). The fringe period decreases with the increase of time separation, but the central fringe location is unchanged. As a comparison, the time shift due to refractive index change, which influence the effective cavity length of the laser, is presented in Fig. 2d-2f, displaying that the change of fringe period is accompanied by fringe location movement by $\varphi = \omega_0 \tau$, a typical feature of DTI-based time sensor[26]. The central fringe location reflects the relative phase φ_{12} in Eq. (1), and the fringe period corresponds to the time separation. Therefore, from the relation of retrieved τ and φ_{12}, we can recognize whether the refractive index and the gain depletion have changed.

Employing the proposed method, the time-separation and relative phase between two long-distance pulses is single-shot revealable, together with the corresponding physical mechanism. Therefore, a quantity of pulse-to-pulse interactions can be single-shot further investigated, like periodic soliton collisions[33], Casimir-like interactions[28], lattice vibration of soliton crystal[34]. Moreover, if the two pulses are the *same pulse* but from adjacent roundtrips, there separation T_{sep} thereby represents the roundtrip time T_r of the pulse. In this way, we can obtain the change of roundtrip time from the interferogram, which has help us to catch the subharmonic entrainment breather soliton[35]. Additionally, the change of roundtrip time and relative phase can reflect somewhat the pulse-to-cavity-parameters interaction, which will help to understand the pulse evolution dynamics of mode-locked laser. In the following, we focus on the pulse buildup and relaxation process to observe the pulse evolution dynamics in a fiber laser.

Experiments. The experimental setup is shown in Fig. 3. The laser cavity incorporates 1.36m erbium-doped fiber (EDF) and 3.46m single mode fiber, so that the total cavity length is 4.82m. The dispersion is 65 ps^2km^{-1} for EDF and -22 ps^2km^{-1} for SMF at 1550nm, indicating a total dispersion of +0.012 ps^2. The laser is mode-locked by nonlinear polarization rotation (NPR) technique[36], facilitated through two polarization controllers (PCs) and a polarization dependent isolator (PDI). The output laser is split into three portions: the first portion (without dispersion) is used to record the instantaneous pulse intensity and serves as the trigger of other two portions, the second portion connects a DTI to detect the relative time and phase of the pulses from adjacent roundtrips, and the third portion is fed into 12km standard single mode fiber (SMF) to carry out the DFT spectral measurement[13]. The DTI is fabricated by two 1:1 optical coupler (OCs), dispersion compensation fiber (DCF) and SMF as extra fibers (EFs), and 12km SMF providing dispersion to time-stretch the pulse pair. The total length of EFs equals to the cavity length and their total dispersion $|\beta_{\text{EFs}}| < 0.0005$ ps^2. Compared with another DTI which contains a delay line in one arm, it can be inferred that the time separation $\tau = T_{diff} - T_r$. The signals are detected by a 10GHz (the first portion) photodetector (PD) and a 40 GHz (the other two portions) PD respectively, and captured by a 10GHz oscilloscope.

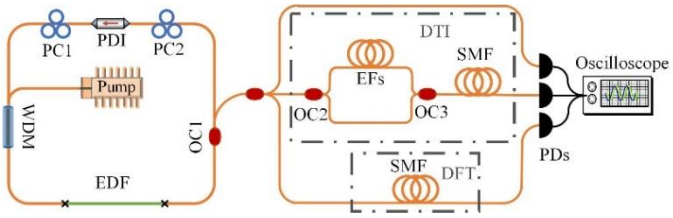

Fig. 3. Experimental setup. The left part is the fiber laser mode-locked by nonlinear polarization rotation, while the right part is the real-time detection system, realizing synchronous measurements of the temporal intensity, spectra, and relative time and phase of adjacent pulses. WDM, wavelength division multiplexer; PDI polarization-dependent isolator; PC, polarization controller; OC, optical coupler; EFs, extra fibers.

Change of roundtrip time during pulse buildup. Our laser is a typical dispersion-managed mode-locked laser[37]. The output pulses exhibit a duration of ~80fs at 1570nm with a repetition rate of 42.8 MHz (Fig. S2). Mode-locking is initiated via tuning on the pump power. The laser can self-start mode-locking operation at 380 mW pump power. Upon the appearance of a pulse signal, it can be triggered and recorded by the oscilloscope. Each data set is recorded over a duration of 2ms and contains about 86000 consecutive pulses. We segment the data into intervals of T_r to obtain a two-dimensional representation of the pulse with one dimension the pulse information within a single roundtrip and the other the pulse evolution over consecutive roundtrips.

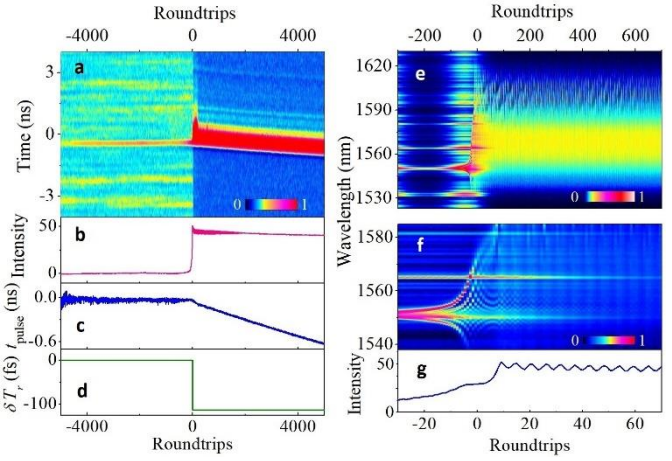

Fig. 4. The buildup of mode-locking. **a** Mode-locking transition detected by the oscilloscope. The recorded time series is segmented with respect to the roundtrip time of the seed fluctuation. **b** Pulse intensity, **c** pulse location and **d** roundtrip time transition during the mode-locking buildup. **e** Spectrum evolution during the transition. **f** A closeup of **e** in 100 roundtrips. **g** Pulse intensity evolution corresponding to **f**.

The timing of the output pulses is precisely defined, which allow to measure the relative roundtrip time change during pulse buildup. The data from undispersed events (Figs. 4a and 4b) show that the mode-locking evolves from seed fluctuation that arises

thousands of roundtrips before the buildup, which has been reported in ref. 13. But here, we focus on the pulse location rather than the pulse spectrum. As shown in Fig. 4a, a clear corner is observed when the pulse buildup. We extract the pulse location in Fig. 4a and obtain the pulse location evolution as shown in Fig. 4c, from which it can be inferred that the roundtrip time of the mode-locked pulse is shorter than that of the seed fluctuation. We have calculated the relative roundtrip time evolution in Fig. 4d, and discovery that a 112-fs reduction of roundtrip time occurs synchronously with the increase of the pulse energy (Fig. 4b). Additionally, other fluctuations exhibit no time drift, indicating their roundtrip time is identical to the seed fluctuation. These phenomena emphasize that the mode-locked pulse has different roundtrip time from the fluctuations.

The DFT technique allows to monitor the evolution of pulse spectrum, in which the interference can reveal the relative of mode-locked pulse and the *beside fluctuation*[13]. Figure 4e displays unambiguous interference fringes within 60 roundtrips after pulse buildup (the corresponding pulse intensity evolution is displayed in Fig. 4g). Together with the roundtrip time reduction shown in Fig. 4d, it can be inferred that the pulse propagates faster than the beside fluctuation. The Kerr effect is eliminated from the reasons for such difference because it slows down the pulse[13] rather than accelerates. Therefore, the pulse acceleration may result from the gain depletion, as illuminated in Fig. 2. Since the intensity of seed fluctuation is much smaller than the pulse, the latter induces much larger gain depletion than the former, which makes the pulse faster than the fluctuations and exhibits as the roundtrip time reduction shown in Fig. 4d. These results reveal that the gain depletion directly influences the roundtrip time of mode-locked laser, and the gain depletion cannot be overlooked for the observation of pulse dynamics.

Relaxation after mode-locking buildup. Employing the DTI technique, the roundtrip time change together with the pulse relative phase evolution can be single-shot monitored after the mode-locking buildup. With this method, three distinct stages, which represent three different physical processes, are observed. The first stage is exhibited in Fig. 5: at the time of pulse buildup, its amplitude oscillates or breathes periodically like breather soliton[20, 35]. The breather period is ~5.5 roundtrips and the ratio of breather amplitude (maximal minus minimal energy) to the average energy is larger than 12% at the beginning. Figures 5a and 5e illustrate the time interferogram evolution during this stage. In the interferograms, both the fringe period and the fringe location change synchronously with the pulse intensity (Figs. 5b and 5f), a peculiar property of breather soliton[35]. We retrieve the time separation τ and relative phase φ using the same method as ref. 27 (Figs. 5c, 5d, 5g, and 5h) and find that both perform like breather soliton: oscillate in a period synchronously with the pulse intensity. The breath attenuates and vanishes over about 1000 roundtrips. The maximum jitter of φ is 0.45π, much smaller than one optical cycle.

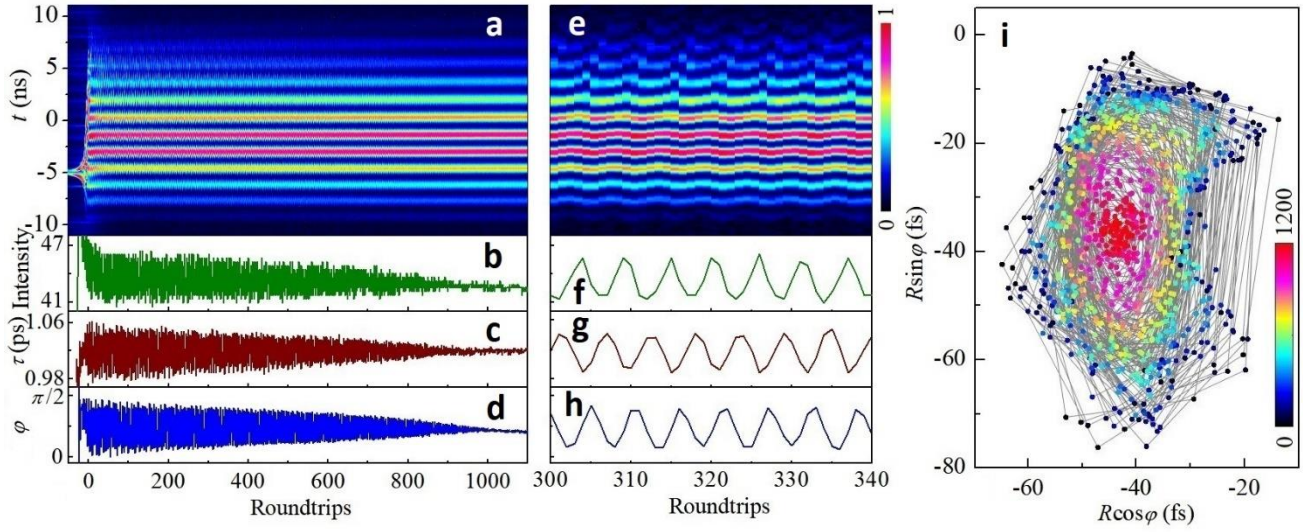

Fig. 5. Breath of mode-locked pulses. **a** Time interferogram evolution measured through DTI. The pulses from adjacent roundtrips are reassembled into soliton pair and stretched into nanosecond, after which their time interferogram arises on oscilloscope. **b** Pulse intensity corresponding to the time interferogram in A. **c** Time separation and **d** relative phase retrieved from **a**. **e-h** Closeup of **a-d**, respectively. **i** Dynamics of the soliton breath mapped into the interaction plane from 0 to 1200 roundtrips.

In principle, the change of refractive index δn introduces linear roundtrip time change δT_r (exhibits as the change of τ in Fig. 5c), which bring the relative phase change of pulses from adjacent roundtrips by $\delta\varphi = 2\pi\delta T_r / T_o$, where T_o is the optical cycle. From Fig. 5d, we can figure out that the maximum roundtrip time jitter is 1.1 fs, while the jitter of retrieved τ is 73fs. Such significant difference can be explained via the gain depletion theory as shown in Fig. 2. Since the pulse advancement is proportion to the degree of gain depletion and the latter is dominated by the pulse intensity[38], the pulse advancement in each roundtrip depends on the pulse intensity. Hence, when the pulse intensity jitters violently, such as breather soliton, the pulse advancement due to gain depletion will vary synchronously, leading to the roundtrip time change. Since such change does not tune the pulse phase as shown in Fig. 2, τ and φ exhibit asynchronous evolution. Hence, the soliton breath stage highlights that the gain depletion can forward the ultrashort pulse, by which the it can affect the timing jitter of the mode-locked lasers[24].

Figure 5i shows the dynamics of the soliton breath mapped into the interaction plane from 10 to 1200 roundtrips, in which the radius represents the time separation τ and the angle is the relative phase φ. The trajectory illustrates the evolution of the laser in the soliton breath stage. The soliton is firstly localized in the outer cycle; with attenuation of the breath, the trajectory moves in, and finally, the system reaches a fixed point, which means the soliton breath vanishes. This can be explained by the change of gain: with the mode-locking buildup, the gain decreases sharply,

as evidenced by the attenuation of other fluctuations in about 100 roundtrips. The gain of the laser cannot support the output of stable soliton, leading to the soliton breath. However, with the attenuation of other fluctuations and the adjustment of the laser, the gain restores gradually, which steady the laser to a fixed point.

To lucubrate the long-term roundtrip time change after mode-locking buildup, we seized the interferograms with different time ranges. The second stage lasts several milliseconds, which requires us to use the ultra-segmentation method with 1us holdoff-time after each shot to monitor the second stage. Figure 6a displays the evolution of time interferogram over 7ms, which contains 7000 shots with 1us interval of adjacent shots. Apparent oscillation of fringe location in a period of ~320 μs can be observed. Like in the soliton breath stage, the corresponding pulse intensity (Fig. 6b) exhibits similar oscillation. Distinguished from the soliton breath stage, the retrieved τ, as depicted in Fig. 6c, presents no oscillation, implying that the roundtrip time change is smaller than the resolution of τ (~5fs). Meanwhile, Fig. 6d shows the relative phase oscillates in the identical period with the pulse intensity, which reveals their interrelation. This synchronization may result from the Kerr effect and/or the refractive index change in the gain medium. Like the breath stage, the oscillation attenuates over time synchronously in intensity and relative phase, implying that the oscillation can be explained by the relaxation oscillation of gain medium, which is ubiquitous in lasers[15].

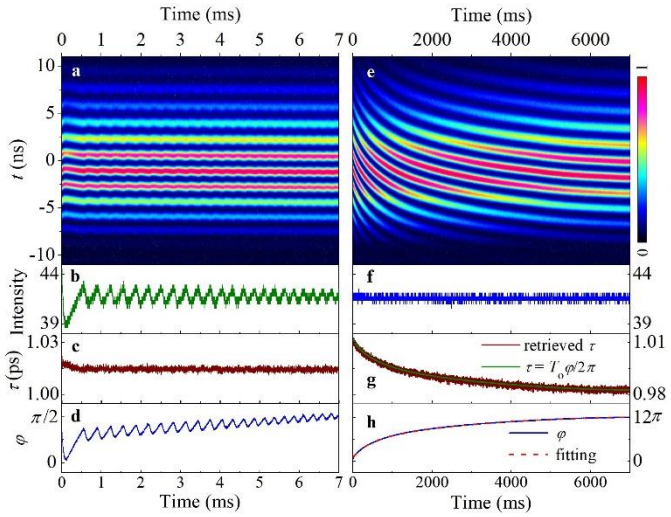

Fig. 6. Long-term relaxation. The left panel is the relaxation oscillation over 7ms, while the right panel refers to the relaxation over 7s. **a**(**e**) Time interferogram evolution over 7ms (7s) after mode-locking buildup. **b**(**f**) pulse intensity, **c**(**g**) time separation, and **d**(**h**) relative phase at the corresponding time of **a**(**e**). We captured one shot per microsecond (millisecond) and 7000 shots was seized.

To further investigate the pulse dynamics, we caught the third stage of the mode-locked laser, the relaxation stage, as presented in Figs. 6e-6h. During this stage, the pulse intensity is changeless, but the time interferogram illustrates an exponentially evolution (Figs. 6e and 6f). Figure 6g displays a total reduction of ~24 fs, meaning the roundtrip time increases by 24 fs. Meanwhile, φ increases synchronously with T_r (Fig. 6h). Also, we calculated τ using $\tau = \tau_0 - T_o(\varphi - \varphi_0)/2\pi$ (τ_0 and φ_0 are the corresponding τ and φ at the time 0) as the olive line in Fig. 6g, which fits well with the retrieved τ. Hence, it is unambiguous that the roundtrip time change owes to the change of refractive index. Whereas, the pulse intensity holds constant from Fig. 6f. Therefore, it can be inferred that the refractive index change originates from the relaxation of gain medium. After the mode-locking buildup, it takes a much longer time than the buildup process for the gain medium to relax to its equilibrium state, during which the change of population inversion reforms the refractive index according to the KK relation. The exponential fitting in Fig. 6h highlights the relaxation process in this laser. Thus, we can give the expression of roundtrip time during the relaxation stage as: $T_r = T_{r0} - T_{rc}\exp(-t/\tau_r)$, where T_{r0} is the roundtrip time after relaxation, T_{rc} is the relaxation coefficient, and τ_r is the relaxation time. In our experiment, the total increment of roundtrip time, namely T_{rc}, is 38fs, and $\tau_r \approx 400$ms. The relaxation time is much longer than the upper-level lifetime (10ms) of EDF[39], which can be explained by the feedback mechanism of the laser.

Discussion

We have time-resolved demonstrated the pulse evolutions and single-shot revealed the pulse-to-cavity-parameters interaction in an ultrafast laser. Using the DTI technique, we have presented the first direct temporal characterization of the pulse relaxation process in mode-locked lasers, on both intensity and roundtrip time. From the relation of retrieved time separation and phase, it is feasible to determine the roles of the refractive index change and the gain depletion change in the change of roundtrip time. With the help of pulse intensity, it is also determinable whether the Kerr effect works. As a typical example, we have revealed that in the pulse breath stage, the main roundtrip time change originates from the gain depletion, and in the relaxation stage, the refractive index change is the source of roundtrip time change. Moreover, the relaxation oscillation and the long-term relaxation demonstrate that the jitter of population reversion level in gain medium can change the roundtrip time in the laser, which should be noticed to reduce the timing jitter in precise timing and frequency comb generation. These may spur new methods to stabilize cavity frequency of mode-locked laser. These results highlight that the DTI can single-shot probe the pulse-to-cavity-parameters interaction, which will tremendously promote the investigation of pulse evolution dynamics in ultrafast lasers, provide new ways to improve the stability of mode-locked lasers, and facilitate the development of ultrafast lasers.

Single-shot probing the time separation and relative phase of the pulse from adjacent roundtrips suggests the applications for DTI on frequency comb, femtosecond pulse synchronization, precise timing, and few-cycle pulse generation. In these areas, the popular method on the feedback control is based on the measurement of repetition frequency and/or the f-to-2f method[40], both of which can only access time-averaged signals. The DTI makes it possible to single-shot monitor the repetition frequency and the phase jitter of mode-locked pulse. Based upon this, it is feasible to carry out all-optical feedback control, which will tremendously promote the development of frequency comb *et. al*. Furthermore, the linear relation between the roundtrip time change and relative phase jitter suggest that when tuning the repetition frequency, the pulse phase will be modulated synchronously. We hope these aspects should attract researchers' attention in the feedback control of frequency comb and precise timing[2,3].

In conclusion, we have demonstrated the application of DTI for tracing the evolution of mode-locked laser. This method provides the first observation of the interplay between pulse and cavity parameters. With this method, we have resolved the evolutions of roundtrip time and pulse relative phase during the buildup process of mode-locking and unveiled the stages of soliton breath, relaxation oscillation, and long-term relaxation after the pulse formation. With the analyzation of roundtrip time change in each stage, we have phenomenologically proved that the gain depletion and the refractive index change are the main origin of the roundtrip time change in fiber laser, and have analyzed their effects on pulse

phases. Moreover, the single-shot measurement of roundtrip time and relative pulse phase is extremely valuable for pulse synthesis, frequency comb and precise timing, and we expect that our method can find further applications in these areas. Furthermore, the DTI technique may have an impact on a wide variety of phenomena of optical soliton, like Casimir-like interaction[28], soliton explosion[18], and soliton molecular breathing[16], and provide new insights into soliton physics.

References

1. Keller, U. Recent developments in compact ultrafast lasers, *Nature* **424**, 831-838 (2003).
2. Xin, M., Safak, K. & Kärtner, F. X. Ultra-precise timing and synchronization for large-scale scientific instruments, *Optica* **5**, 1564-1578 (2018).
3. Picqué, N. & Hänsch, T. W. Frequency comb spectroscopy, *Nat. Photonics* **13**, 146-157 (2019).
4. Krylov, A. A., Chernykh, D. S. & Obraztsova, E. D. Gyroscopic effect detection in the colliding-pulse hybridly mode-locked erbium-doped all-fiber ring soliton laser, *Opt. Lett.* **42**, 2439-2442 (2017).
5. Krolopp, Á., Csákányi, A., Haluszka, D., Csáti, C., Vass, L., Kolonics, A., Wikonkál, N. & Szipőcs, R. Handheld nonlinear microscope system comprising a 2 MHz repetition rate, mode-locked Yb-fiber laser for in vivo biomedical imaging, Biomed. *Opt. Express* **7**, 3531-3542 (2016).
6. Luo, H., Zhan, L., Zhang, L., Wang, Z., Gao, C. & Fang, X. Generation of 22.7-fs 2.8-nJ pulses from an erbium-doped all-fiber laser via single stage soliton compression, *J. Lightwave Technol.* **35**, 3780-3784 (2017).
7. Morgner, U. et al. Sub-two-sycle pulses from a Kerr-lens mode-locked Ti:sapphire laser, *Opt. Lett.* **24**, 411-413 (1999).
8. Grelu, P. & Akhmediev, N. Dissipative solitons for mode-locked lasers, *Nat. Photonics* **6**, 84-92 (2012).
9. Grelu, P. (ed.) *Nonlinear Optical Cavity Dynamics: From Microresonators to Fiber Lasers* (Wiley, Berlin, Germany, 2016).
10. Pu, N., Shieh, J., Lai, Y. & Pan, C. Starting dynamics of a cw passively mode-locked picosecond Ti:sapphire/DDI laser, *Opt. Lett.* 20, 163-165 (1995).
11. Li, H., Ouzounov, D. G. & Wise, F. W. Starting dynamics of dissipative-soliton fiber laser, *Opt. Lett.* **35,** 2403-2405 (2010).
12. Lecaplain, C., Grelu, P., Soto-Crespo, J. M. & Akhmediev, N. Dissipative rogue waves generated by chaotic pulse bunching in a mode-locked laser. *Phys. Rev. Lett.* **108**, 233901 (2012).
13. Herink, G., Jalali, B., Ropers, C. & Solli, D. R. Resolving the build-up of femtosecond mode-locking with single-shot spectroscopy at 90 MHz frame rate, *Nat. Photonics* **10**, 321-326 (2016).
14. Liu, X., Yao, X. & Cui, Y. Real-time observation of the buildup of soliton molecules, *Phys. Rev. Lett.* **121**, 023905 (2018).
15. Liu, X., Popa, D. & Akhmediev, N. Revealing the transition dynamics from Q switching to mode locking in a soliton laser, *Phys. Rev. Lett.* **123**, 093901 (2019).
16. Herink, G., Hurtz, F., Jalali, B., Solli, D. R. & Ropers, C. Real-time spectral interferometry probes the internal dynamics of femtosecond soliton molecules, Science **356**, 50-54 (2017).
17. Krupa, K., Nithyanandan, K., Andral, U., Tchofo-Dinda, P. & Grelu, P. Real-time observation of internal motion within ultrafast dissipative optical soliton molecules, *Phys. Rev. Lett.* **118**, 243901 (2017).
18. Runge, A. F. J., Broderick, N. G. R. & Erkintalo, M. Observation of soliton explosions in a passively mode-locked fiber laser, *Optica* **2**, 36-39 (2015).
19. Peng, J. & Zeng, H. Experimental observations of breathing dissipative soliton explosions, *Phys. Rev. Appl.* **12**, 034052 (2019).
20. Peng, J., Boscolo, S., Zhao, Z. & Zeng, H. Breathing dissipative solitons in mode-locked fiber lasers, *Sci. Adv.* **5**, eaax1110 (2019).
21. Apolonski, A. et al. Controlling the phase evolution of few-cycle light pulses, *Phys. Rev. Lett.* **85**, 740-743 (2000).
22. Shelton, R. K., Ma, L. S., Kapteyn, H. C., Murnane, M. M., Hall, J. L. & Ye, J. Phase-coherent optical pulse synthesis from separate femtosecond lasers, *Science* **293**, 1286-1289 (2001).
23. Schibli, T. R., Hartl, I., Yost, D. C., Martin, M. J., Marcinkevičius, A. & Fermann, M. E. Optical frequency comb with submillihertz linewidth and more than 10 W average power, *Nat. Photonics* **2**, 355-359 (2008).
24. Kim, J. Cox, J. A. Chen, J. & Kärtner, F. X. Drift-free femtosecond timing synchronization of remote optical and microwave sources, *Nat. Photonics* **2**, 733-736 (2008).
25. Hecht, E. *Optics* (Pearson Education, Global Edition, 2017).
26. Xian, T., Zhan, L., Zhang, W., Zhang, W. & Gao, L. Single-shot detection time-stretched interferometer with attosecond precision, in *optical fiber communication conference (OFC), San Diego, CA, 2020*, paper M1C.4.
27. Kutz, J. N., Collings, B. C., Bergman, K. & Knox, W. H. Stabilized pulse spacing in soliton lasers due to gain depletion and recovery, *J. Quantum Electron.* **34**, 1749-1757 (1998).
28. Sulimany, K. et al. Bidirectional soliton rain dynamics induced by Casimir-like interaction in a graphene mode-locked fiber laser, *Phys. Rev. Lett.* **121**, 133902 (2018).
29. Janos, M. & Guy, S. C. Signal-induced refractive index changes in erbium-doped fiber amplifiers, *J. Lightwave Technol.* **16**, 542-548 (1998).
30. Boyd, R. W. *Nonlinear optics* (Elsevier, Singapore, 2009).
31. Haus, H. A. Theory of mode locking with a slow saturable absorber, IEEE *J. Quantum Electron.* **11**, 736-746 (1975).
32. Gumenyuk, R. V., Korobko, D. A. & Zolotovskii, I. O. Stabilization of passive harmonic mode-locking in a fiber ring laser, *Opt. Lett.* **45**, 184-187 (2020).
33. Roy, V., Olivier, M., Babin, F. & Piché, M. Dynamics of periodic pulse collisions in a strongly dissipative-dispersive system, *Phys. Rev. Lett.* **94**, 203903 (2005).
34. Cole, D. C., Lamb, E. S., Del'Haye, P., Diddams, S. A. & Papp, S. B. Soliton crystals in Kerr resonators, *Nat. Photonics* **10**, 671-676 (2017).
35. Xian, T., Zhan, L., Wang, W., & Zhang, W. Subharmonic entrainment breather solitons in ultrafast lasers, *Phys. Rev. Lett.* **125**, 163901 (2020).
36. Komarov, A., Leblond, H. & Sanchez, F. Theoretical analysis of the operating regime of a passively-mode-locked fiber laser through nonlinear polarization rotation, *Phys. Rev. A* **72**, 063811 (2005).
37. Deng, D., Zhan, L., Gu, Z., Gu, Y. & Xia, Y. 55-fs pulse generation without wave-breaking from an all-fiber Erbium-doped ring laser, *Opt. Express* **17**, 4284-4288 (2009).
38. Weill, R., Bekker, A., Smulakovsky, V., Fischer, B. & Gat, O. Noise-mediated Casimir-like pulse interaction mechanism in lasers, *Optica* **3**, 189-192 (2016).
39. Zareanborji, A., Yang, H., Town, G. E., Luo, Y. & Peng, G. Simple and accurate fluorescence lifetime measurement scheme using traditional time-domain spectroscopy and modern digital signal processing, *J. Lightwave Technol.* **34**, 5033-5043 (2016).
40. Rossi, G. M. et. al. Sub-cycle millijoule-level parametric waveform synthesizer for attosecond science, *Nat. Photonics* **14**, 629-635 (2020).

Acknowledgements

The authors acknowledge the support from the National Natural Science Fund of China (11874040), and the Foundation for leading talents of Minhang, Shanghai.

Author contributions

T. X. and L. Z. conceived the idea of dispersive temporal interferometer and constructed the theoretical model. T. X. performed the experiment. All authors analyzed the data and wrote the manuscript.

Data availability

All data needed to evaluate the conclusions in the paper are present in the paper and/or the Supplementary Materials. Additional data related to this paper may be requested from L. Z. (lizhan@sjtu.edn.cn).

Competing interests: The authors declare that they have no competing interests.

Figures

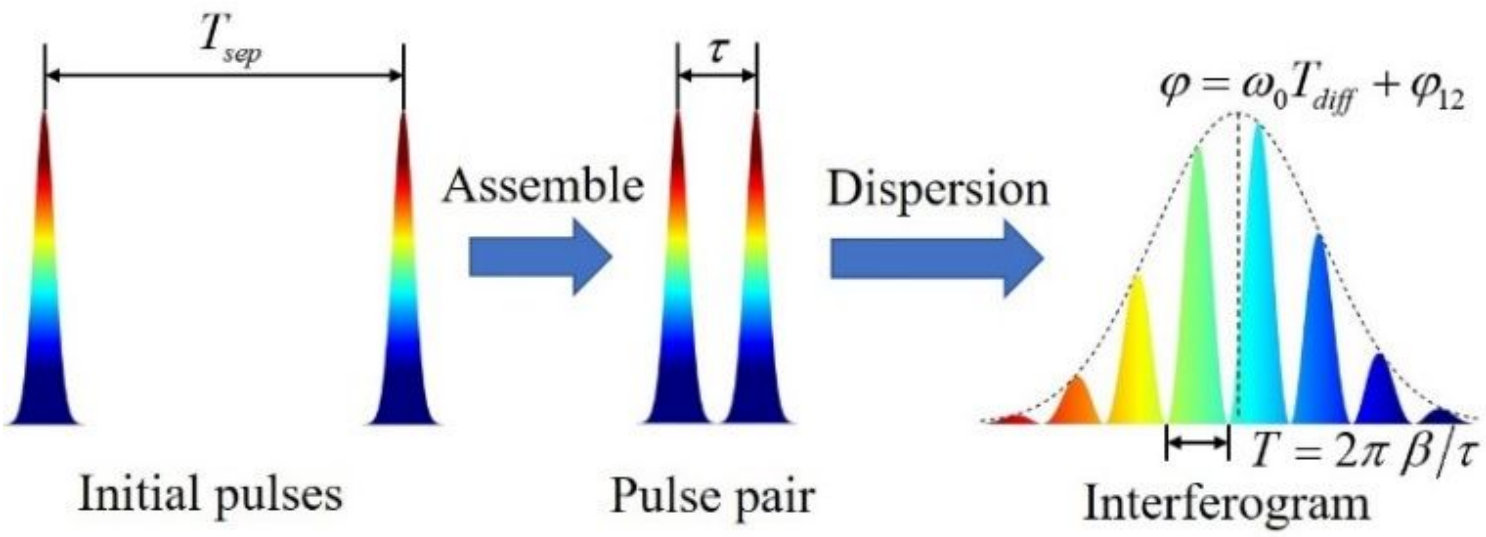

Figure 1

Concept of capturing the interaction of different pulses with DTI.

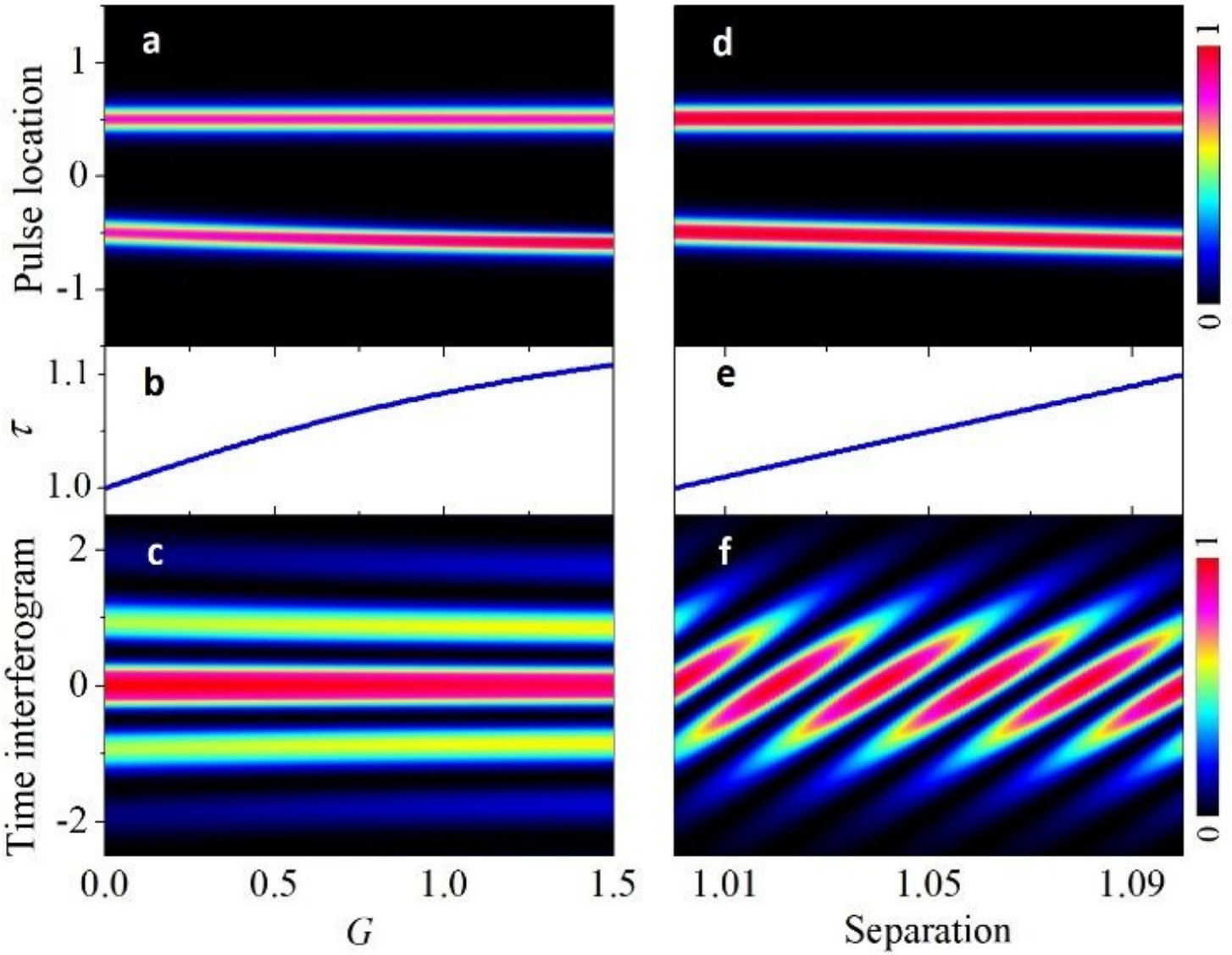

Figure 2

Time shift of mode-locked pulses due to time-dependent gain (left panel) and refractive index change (right panel). a(d) pulse relative location. The upper is the reference pulse that has a fix location, and the lower is the signal pulse. b(e) relative time separation of the pulses in a(d). c(f) time interferogram evolution of the pulses in a(d).

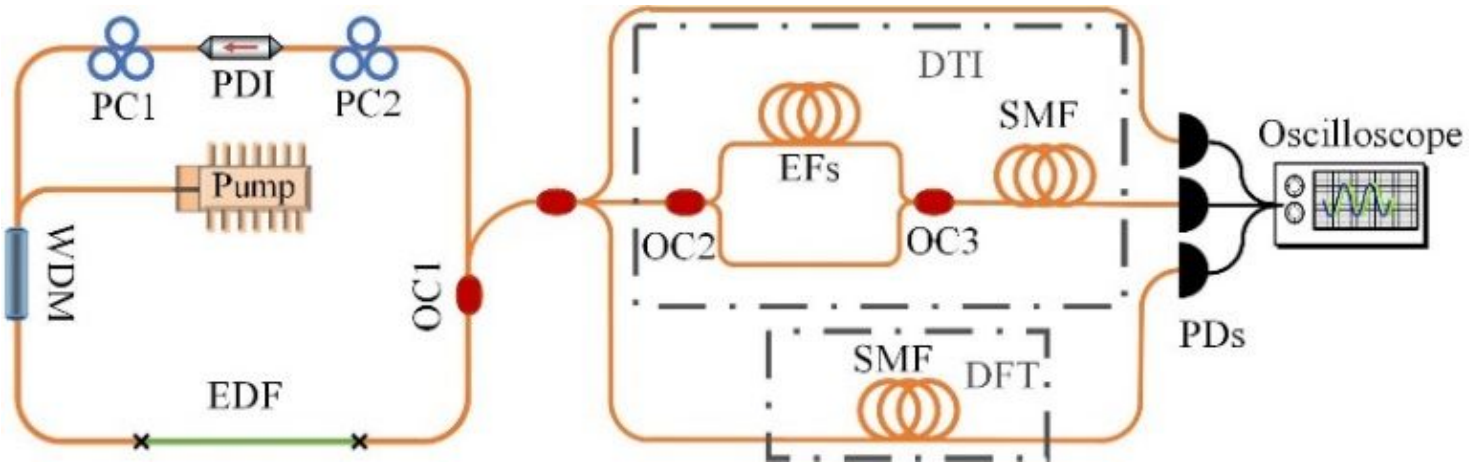

Figure 3

Experimental setup. The left part is the fiber laser mode-locked by nonlinear polarization rotation, while the right part is the real-time detection system, realizing synchronous measurements of the temporal intensity, spectra, and relative time and phase of adjacent pulses. WDM, wavelength division multiplexer; PDI polarization-dependent isolator; PC, polarization controller; OC, optical coupler; EFs, extra fibers.

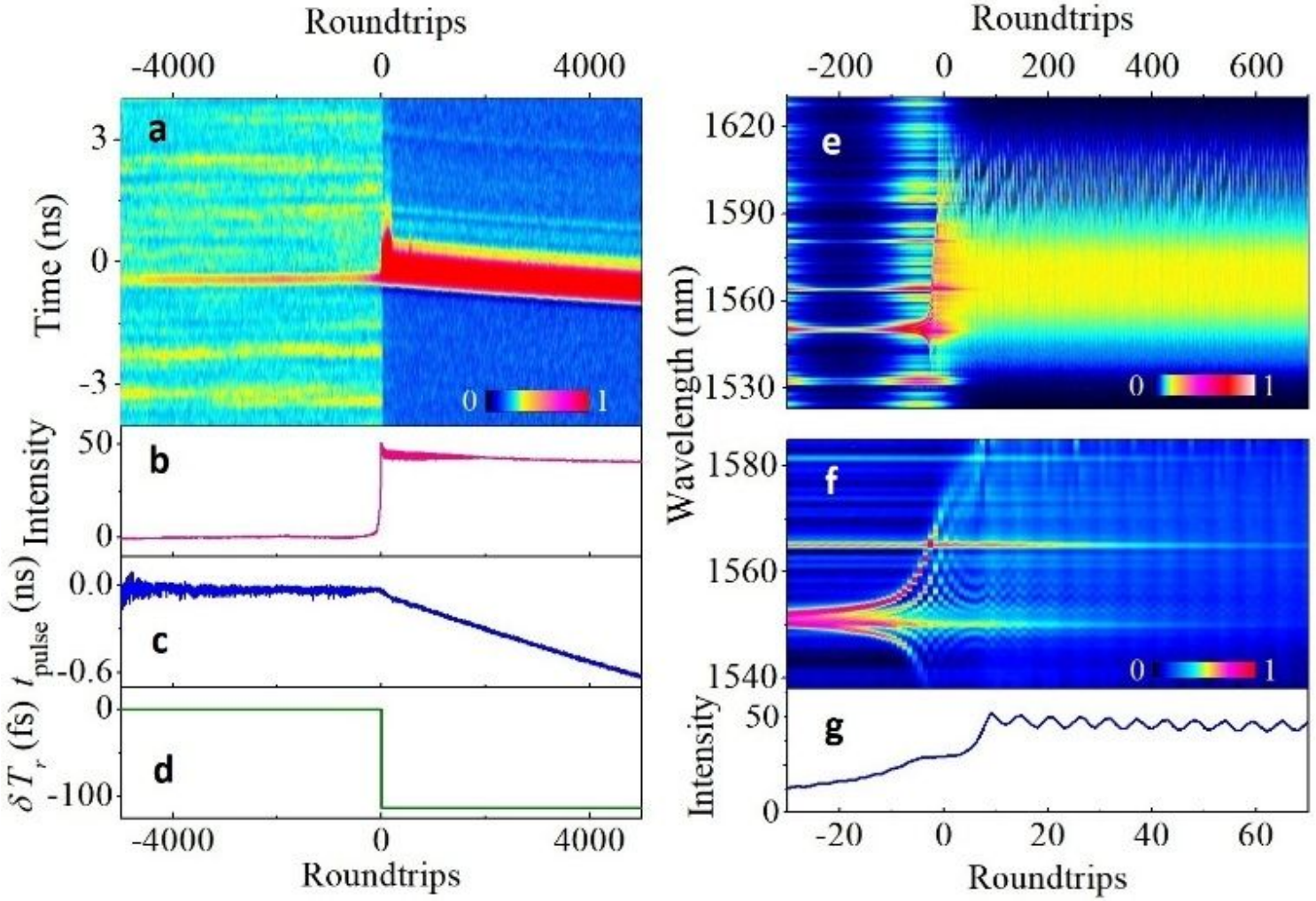

Figure 4

The buildup of mode-locking. a Mode-locking transition detected by the oscilloscope. The recorded time series is segmented with respect to the roundtrip time of the seed fluctuation. b Pulse intensity, c pulse location and d roundtrip time transition during the mode-locking buildup. e Spectrum evolution during the transition. f A closeup of e in 100 roundtrips. g Pulse intensity evolution corresponding to f.

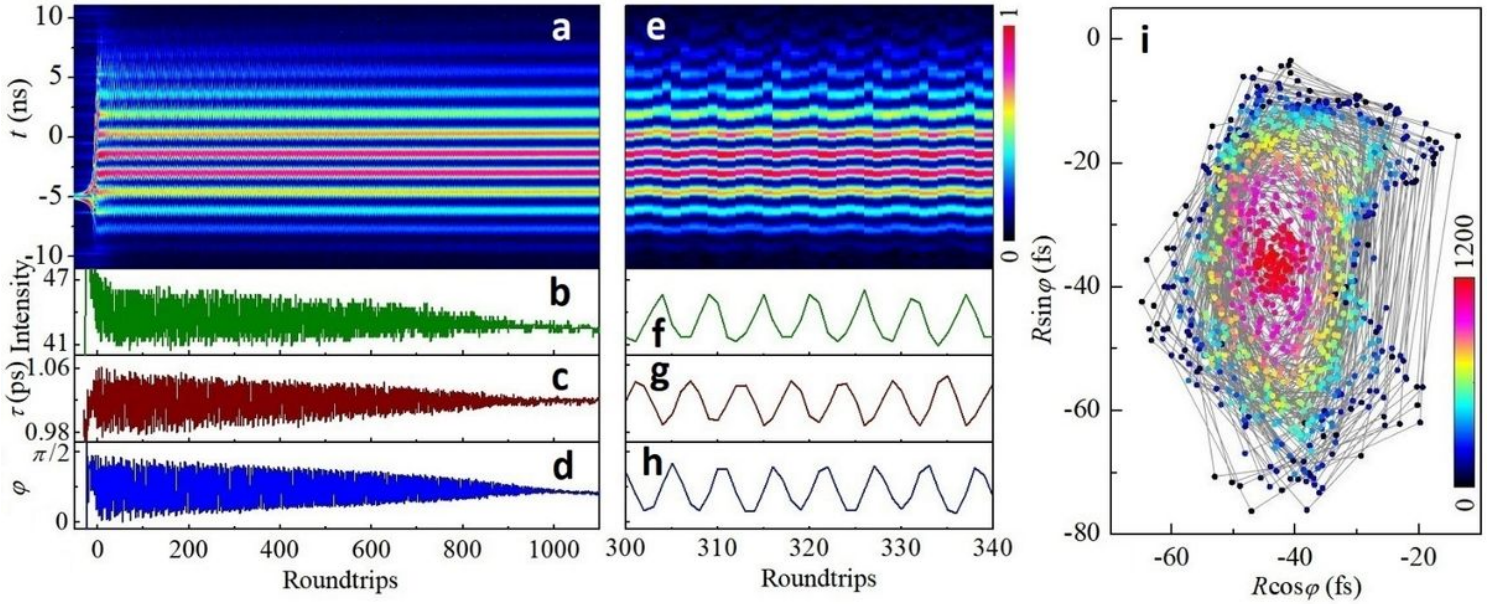

Figure 5

Breath of mode-locked pulses. a Time interferogram evolution measured through DTI. The pulses from adjacent roundtrips are reassembled into soliton pair and stretched into nanosecond, after which their time interferogram arises on oscilloscope. b Pulse intensity corresponding to the time interferogram in A. c Time separation and d relative phase retrieved from a. e-h Closeup of a-d, respectively. i Dynamics of the soliton breath mapped into the interaction plane from 0 to 1200 roundtrips.

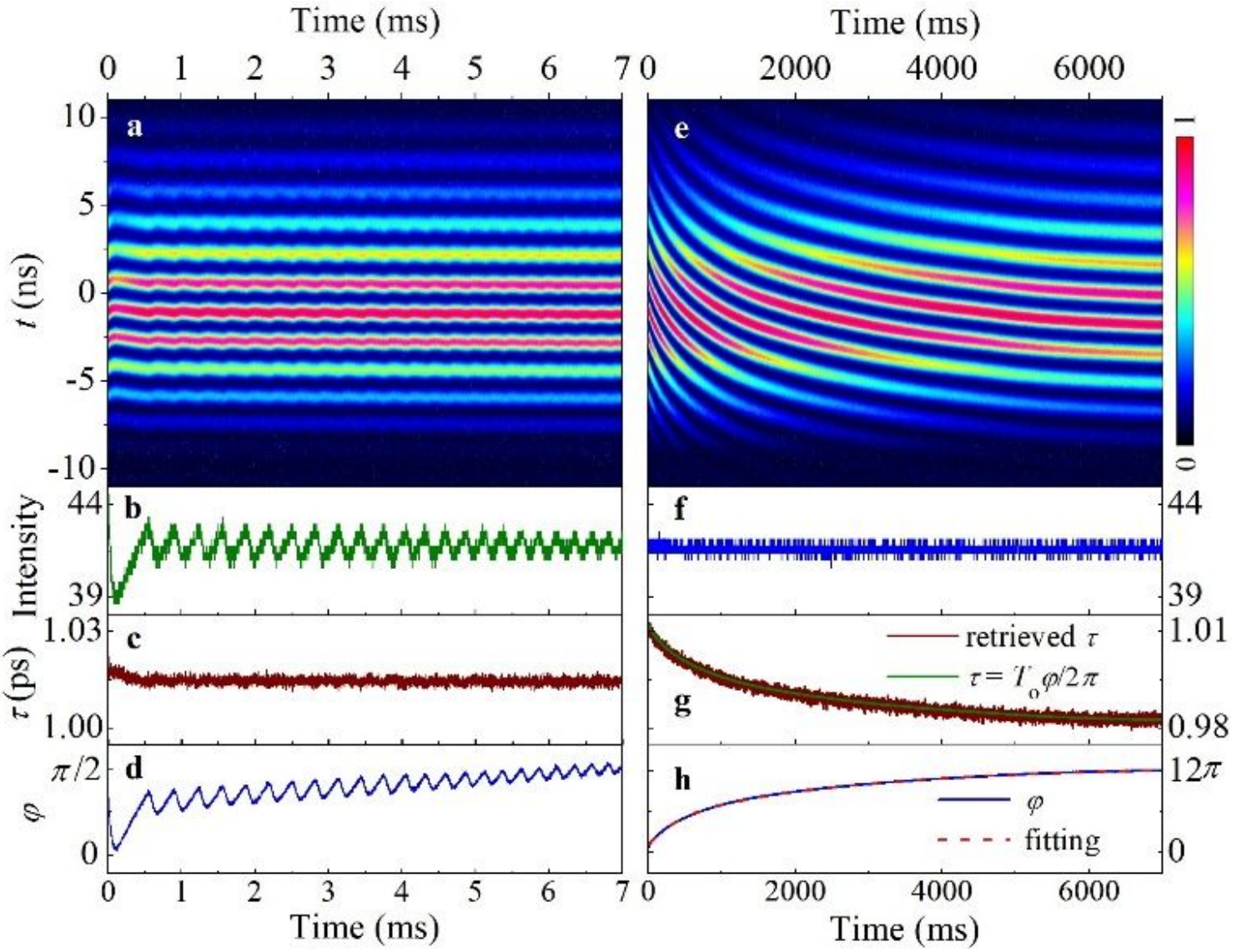

Figure 6

Long-term relaxation. The left panel is the relaxation oscillation over 7ms, while the right panel refers to the relaxation over 7s. a(e) Time interferogram evolution over 7ms (7s) after mode-locking buildup. b(f) pulse intensity, c(g) time separation, and d(h) relative phase at the corresponding time of a(e). We captured one shot per microsecond (millisecond) and 7000 shots was seized.

Supplementary Files

This is a list of supplementary files associated with this preprint. Click to download.

- XTHNCsupplementmaterial.docx